drones

MDPI

Article

Towards Mobile Wind Measurements Using Joust Configured Ultrasonic Anemometer for Applications in Gas Flux Quantification

Derek Hollenbeck [1], Colin Edgar [2], Eugenie Euskirchen [2] and Kristen Manies [3,*]

[1] Department of Mechanical Engineering, University of California–Merced, Merced, CA 95343, USA; dhollenbeck@ucmerced.edu
[2] Institute of Arctic Biology, University of Alaska–Fairbanks, Fairbanks, AK 99775, USA; cedgar3@alaska.edu (C.E.); seeuskirchen@alaska.edu (E.E.)
[3] U.S. Geological Survey, Moffett Field, CA 94035, USA
* Correspondence: kmanies@usgs.gov

Abstract: Small uncrewed aerial systems (sUASs) can be used to quantify emissions of greenhouse and other gases, providing flexibility in quantifying these emissions from a multitude of sources, including oil and gas infrastructure, volcano plumes, wildfire emissions, and natural sources. However, sUAS-based emission estimates are sensitive to the accuracy of wind speed and direction measurements. In this study, we examined how filtering and correcting sUAS-based wind measurements affects data accuracy by comparing data from a miniature ultrasonic anemometer mounted on a sUAS in a *joust configuration* to highly accurate wind data taken from a nearby eddy covariance flux tower (aka the Tower). These corrections had a small effect on wind speed error, but reduced wind direction errors from 50° to >120° to 20–30°. A concurrent experiment examining the amount of error due to the sUAS and the Tower not being co-located showed that the impact of this separation was 0.16–0.21 ms^{-1}, a small influence on wind speed errors. Lower wind speed errors were correlated with lower turbulence intensity and higher relative wind speeds. There were also some loose trends in diminished wind direction errors at higher relative wind speeds. Therefore, to improve the quality of sUAS-based wind measurements, our study suggested that flight planning consider optimizing conditions that can lower turbulence intensity and maximize relative wind speeds as well as include post-flight corrections.

Keywords: wind measurement; multirotor; sUAS; flux quantification

check for updates

Academic Editor: Eben N. Broadbent

Received: 12 November 2024
Revised: 11 January 2025
Accepted: 15 January 2025
Published: 26 January 2025

Citation: Hollenbeck, D.; Edgar, C.; Euskirchen, E.; Manies, K. Towards Mobile Wind Measurements Using Joust Configured Ultrasonic Anemometer for Applications in Gas Flux Quantification. *Drones* **2025**, *9*, 94. https://10.3390/drones9020094

Copyright: © 2025 by the authors. Licensee MDPI, Basel, Switzerland. This article is an open access article distributed under the terms and conditions of the Creative Commons Attribution (CC BY) license (https://creativecommons.org/licenses/by/4.0/).

1. Introduction

The Intergovernmental Panel on Climate Change (IPCC) has stated that recent increases in global temperatures are human caused. The dominant causes of this warming are increases in greenhouse gases (GHGs) such as carbon dioxide (CO_2) and methane (CH_4) [1]. In the United States, the majority of these emissions are from transportation (28%), electricity production (25%), and industry (23%) [2]. In order to combat climate change, land managers must first understand how individual GHG sources contribute to these emissions. A variety of techniques are used to measure the source and magnitude of these gas fluxes to the atmosphere, including satellites, airborne campaigns, and ground-based techniques. Due to their maneuverability and low-altitude capabilities, small uncrewed aerial systems (sUASs) have also recently been used to measure gas emissions and fluxes.

sUASs have been used to help quantify GHG emissions from a variety of sources [3–5]. For example, Gullett et al. [6] measured the nitrogen oxide (NO), nitrogen dioxide (NO_2),

carbon dioxide (CO_2), and carbon monoxide (CO) being emitted from natural gas boiler stack plumes. Their sUAS-based measurements were within 0.8–7.8% of values measured by continuous emission monitoring systems (CEMSs). sUASs have also been used to examine emissions from oil and gas infrastructure [7–10], landfills [11–13], as well as ozone concentrations [14,15]). sUAS-based measurements can be very useful in situations where monitoring emissions is potentially hazardous, such as measuring volcano plumes [16–18] and wildfire emissions [19,20], or where the location of interest is difficult to access (i.e., no roads). The ability of sUASs to quantify GHG emissions from natural sources, such as wetlands, is also of interest [21].

Early experiments examining the ability of sUASs to measure wetland methane emissions found that although the magnitude of these emissions were similar to eddy covariance flux tower measurements, sUAS-based fluxes were sensitive to wind data [22]. This sensitivity stems from the fact that sUAS-based emission estimates are directly proportional to the wind measurements. As such, when wind measurements are off, emission errors can increase by a factor proportional to the true wind speed error. In [23], uncertainties in methane emission quantification with sUAS were explored against OTM-33A [24]. The authors explored variations in the way the spatial methane measurements were interpolated and how the wind components were applied to the measurements (i.e., scalar, logarithmic, and projected). In brief, they found that cluster-based kriging outperformed ordinary kriging. However, their emission results still showed uncertainty levels of 30–77% [23], the variability of which was in part driven by whether the flight occurred during optimal vs sub-optimal wind conditions. They also found that wind speeds below 2.3 ms^{-1} showed increased errors in flux measurement, further emphasizing the importance of wind measurements.

Measuring wind data from sUAS has been achieved utilizing on-board ultrasonic anemometers (UAs) [25,26], five-hole probes [27,28], as well as by using the inertial measurement unit (IMU) of the aircraft [27,29]. With IMU-based techniques, the sUAS accelerometer and gyroscope data are used (in conjunction with the GPS and altitude measurements) to estimate the wind. While the IMU approach requires no additional instrumentation, this method requires intimate knowledge of the aircraft's aero-mechanical features for computing drag components, as well as knowledge of power requirements as a function of pitch and roll commands (requiring wind tunnel testing for highly accurate values) [30]. When sensors are used to measure wind data, placement of these sensors is important. For example, a five-hole probe sensor has a cone of acceptance of approximately $\pm 45°$ relative to the aircraft heading for which the wind can be measured [27], and, as such, this sensor must be placed on the front of an aircraft. Other wind sensors, such as ultrasonic anemometers, can be placed in front of or be mounted directly above the aircraft [25,30]. In order to minimize the affect from the rotors, they need to be placed at a distance of 1.5 rotor diameters or greater [26] to allow for free stream airflow into the sensing region.

Measuring gases and winds simultaneously requires integration of the gas and wind sensors such that theses sensors do not interfere with one another nor impact the performance of the sUAS. To reduce mounting hardware and weight, these instruments are often mounted together, sometime along a boom situated such that the instruments are located in front of the sUAS in a *joust configuration* . It can be argued that this configuration may allow for better airflow into both sensors given the aircraft orientation is pointed predominately into the wind [31].

The purpose of this study was to examine how wind measurements taken from joust-configured sUASs during a mission to calculate gas (methane) fluxes compare to two sets of ground-based wind measurements. We applied various levels of corrections (e.g., translation- and rotation-induced velocities) to determine key sources of error given

different measurement scenarios. The paper is organized as follows: in Section 2, the experimental site, sampling approach, and data corrections/filtering are outlined; Section 3 showcases the results between the two sets of ground-based sensors as well as how the sUAS-based data vary with filters/corrections for sUAS movement (speed, headings, and rotation) and angle differences between the sUAS heading and mean wind direction or sUAS direction of travels; Section 4 discusses our findings and provides suggestions for obtaining more accurate wind speed and direction measurements; and Section 5 gives some concluding remarks.

2. Materials and Methods

2.1. Experiment Site

This study took place in the Alaska Peatland Experiment (APEX), located within the lowlands of the Bonanza Creek Long-term Ecological Research (LTER) site, in Interior Alaska. SUAS flights were conducted within a collapse scar bog (~2000 m^2) along the flight lines shown in Figure 1. This bog formed from recent permafrost thaw and is surrounded by forested peat plateaus that still contain permafrost (aka frozen soil [32]). Bog vegetation is characterized by diverse *Sphagnum* and *Carex* spp. plants. This bog has an eddy covariance flux tower [33] measuring carbon and energy fluxes as well as wind data. The sUAS was flown in August when methane flux was expected to be near its maximum. For the time period of these flights (9–11 August 2022, between 11:00 and 19:00), the average temperature was 21.2 °C (std dev = 3.9, range = 13.9–28.8 °C, data measured by the onboard methane sensor, RKI Instruments), the average pressure was 995.6 mb (std dev = 1.6, range = 995.6–1001.8 mb, RKI Instruments), and the average relative humidity was 40% (range = 30–55%; Fairbanks Airport, https://www.ncdc.noaa.gov/(accessed on 6 January 2025)). At this site, the wind predominately comes from the northeast and southwest.

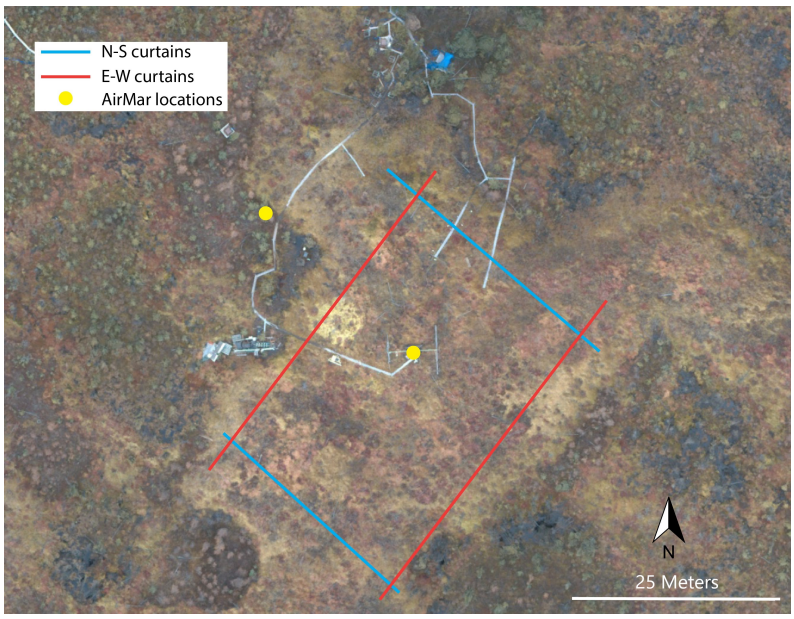

Figure 1. Overview of the bog with locations marked for the two sets of curtains flown (depending on dominant wind direction, red and blue lines) and the AirMar 200WX WeatherStation (yellow dots). The Tower is located within the flight curtains at the same location as noted for the AirMar. Also visible in this image are the boardwalks providing access to this site. Landscape imagery courtesy of J. Hollingsworth, Bonanza Creek LTER, 2019.

2.2. Aerial-Based Sampling Approach

We placed a TriSonica miniature ultrasonic anemometer (Anemoment, Longmont, CO, USA) on a Matrice 600 (M600; DJI, Shenzhen, China), which we refer to as the TriSonica. This instrument was mounted at the end of a carbon fiber boom such that it was 99 cm in front of the center of the M600 (Figure 2). This placement was chosen to minimize the effects of propeller wash on wind speed, wind direction, and methane measurements [31,34–36]. One of the main applications of these flights was to estimate methane flux, or the rate of methane emissions from the bog, using the mass balance method [7]. When a gas plume is being advected from a source in a single direction, flux can be typically be captured using only a single downwind curtain (as long as it encapsulates the plume). A curtain consists of multiple linear transects at various altitudes, typically with equal vertical spacings, which span the area where the plume is expected. An upwind curtain is often used to either verify that there is no additional gas entering from upwind of the source area or, if there is an upwind source, to quantify those background levels. If one orients these curtains approximately perpendicular to the dominant wind direction, one can assume there is little to no flux leaving the site from the unmeasured sides and only fly from these upwind and downwind positions. In our study, the wind direction changed at times, creating two sets of upwind/downwind curtains (four flights each), which we labeled north/south (N-S) and east/west (E-W) according to the dominate wind direction (Figure 1). Transects within a curtain ranged from altitudes of approximately 2 to 20 m (AGL). During periods of measurement, the boom of the sUAS was pointed in the direction of travel. Once a transect was completed, the sUAS would climb in altitude $\approx$ 2 m and rotate until it was facing the direction of travel again. These flights were flown near an eddy covariance flux tower (aka Tower) to allow comparisons between the sUAS- and Tower-based wind and flux measurements.

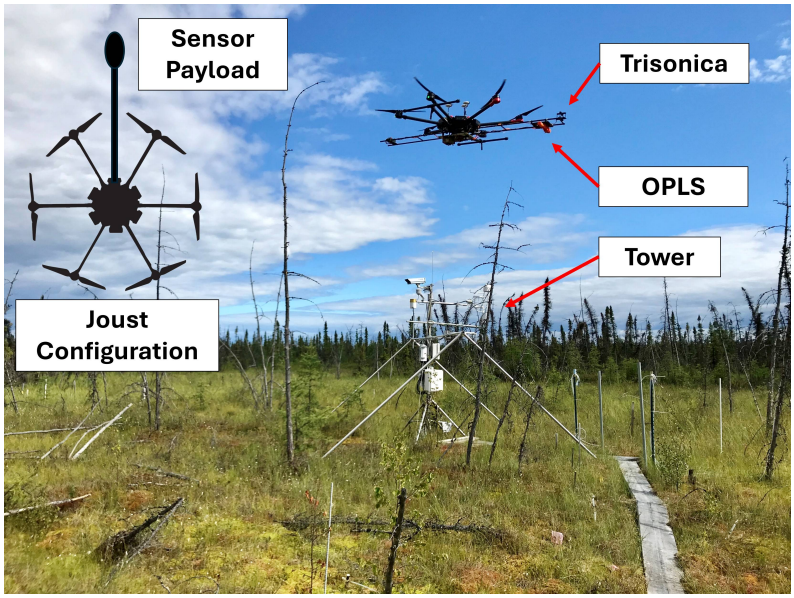

Figure 2. Photograph of Matrice 600 with TriSonica mini anemometer mounted on boom flying in Alaskan bog that also has eddy covariance flux tower (aka the Tower). An open path laser system (OPLS) noted measures methane. Photograph used with permission, J. Jonas, NASA.

2.3. Ground-Based Sampling Approach

In this work, we utilized two different ground-based sensors. The first is the eddy covariance tower (aka the Tower) which is reserved as the gold standard in this study. The second is a low-cost and portable solution that is easily deployed to different locations on the site, referred to as AirMar. Both are described in more detail below.

2.3.1. Tower

The Tower wind data, $\mathbf{u}_\tau(t) = [u_{\tau1}, u_{\tau2}, u_{\tau3}]^T$, were measured using a 3D sonic anemometer (CSAT-3; Campbell Scientific Instruments, Logan, UT, USA) at ≈ 3 m above ground. The stated resolution for this instrument is 1 mms^{-1} root mean square (ux, uy) and 0.5 mms^{-1} root mean square (uz) with wind direction accuracy of $\pm 0.7°$at 1 ms^{-1} for horizontal wind (https://www.campbellsci.com/csat3 (accessed on 6 January 2025)). For these measurements, 0 degrees north corresponded to 160 degrees (i.e., $\phi_T = 160$), such that these data needed to be adjusted prior to data comparisons. The Tower data were sampled at a rate of 10 Hz.

2.3.2. AirMar

The AirMar 200WX WeatherStation (AirMar Technology Corporation, Milford, NH, USA) was mounted on a tripod, such that measurements, $\mathbf{u}_a(t) = [u_{a1}, u_{a2}, u_{a3}]^T$, were taken 232 cm above the ground level. Because the AirMar is a 2D sensor, there are no data in the third dimension, such that $(u_{a3} = 0\ \forall t)$. We used this instrument as a mobile sensor to investigate the potential effects of non-collocation on wind measurement. Therefore, at times, this instrument was located alongside the Tower, while at other times it was placed at the edge of the bog within the forested peat plateau (Figure 1). This AirMar unit has a documented wind speed accuracy of 0.15 ms^{-1} and a stated wind direction accuracy of $\pm 3°$at 10 ms^{-1} (https://www.airmar.com/Product/200WX (accessed on 6 January 2025)). The AirMar sensor outputs data at 2 Hz as wind angle, with 0 degrees being the direction in which the sensor is pointed, and wind speed (in knots). At each location the AirMar was deployed, the sensor was aligned to magnetic north using a compass; therefore, data were converted to true north using the magnetic variation for this region of 15.92° (https://www.ngdc.noaa.gov/geomag/calculators/magcalc.shtml (accessed on 5 November 2024)).

2.4. Data Post-Processing

To effectively conduct an inter-comparison between the TriSonica (or aerial-based data) and the land-based measurements (Tower and AirMar), each dataset needed some processing, filtering, and/or corrections. First, because the sampling frequency and timing for each instrument were different, for each analysis, a target frequency was chosen and data were interpolated as needed to this timing. For the inter-comparison between the Tower and AirMar, the sample frequency was 2 Hz. For the comparison between the Tower and the aerial-based measurements, it was 5 Hz.

In addition, each instrument had a different orientation and/or coordinate system (Figure 3). Therefore, each dataset needed to be aligned (spatially). Below we discuss this process for each component of our system.

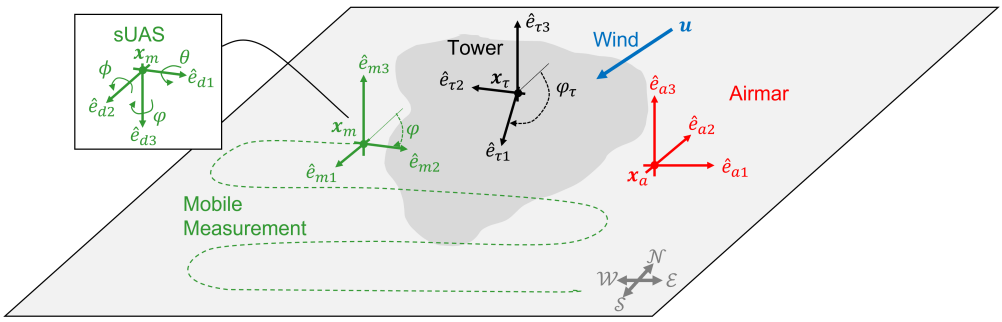

Figure 3. The coordinates used for the different wind instruments and the sUASs are shown here. Because each system used different orientations, the data first needed to be aligned, as described in Section 2.4.1.

2.4.1. sUAS Corrections

The TriSonica was mounted on the boom such that the north orientation was facing the front of the aircraft (i.e., the direction of flight). First, we needed to ensure that the TriSonica's basis vectors, $\hat{\mathbf{e}}_m(t) = [\hat{e}_{m1}, \hat{e}_{m2}, \hat{e}_{m3}]^T$, were aligned with the basis vectors of the M600's body fixed frame coordinates, $\hat{\mathbf{e}}_d(t) = [\hat{e}_{d1}, \hat{e}_{d2}, \hat{e}_{d3}]^T$, where t is time (see Figure 3). For example, a positive value for $\hat{e}_{d3}$ of the M600 is pointed towards the ground (https://developer.dji.com/mobile-sdk/documentation/introduction/flightController_concepts.html (accessed on 21 January 2025)), in contrast to the TriSonica anemometer, where a positive value of $\hat{e}_{m3}$ is pointed away from the ground. Therefore, the first step in our data processing was to align the TriSonica data to the M600 coordinate system so that we could correct the TriSonica data according to the M600 direction of flight (or yaw), pitch, and roll. Positional data from the M600 were recorded in terms of true north based on the onboard GPS system.

As the sUAS is moving during measurements, the wind sensor is experiencing fluctuations due to local turbulence, propeller effects, and induced effects from sUASs. To understand the degree to which sUAS orientation was influencing the measurements, we adjusted the measured TriSonica data, $\mathbf{u}_m(t)$, based on the M600 data, for both translation $[\mathbf{v}(t)]$ and rotation $[\dot{\Omega}(t)]$, where $\Omega = [\phi, \theta, \varphi]^T$. To achieve this, we utilized the following rotation matrices:

$$R_\phi = \begin{bmatrix} 1 & 0 & 0 \\ 0 & \cos\phi & -\sin\phi \\ 0 & \sin\phi & \cos\phi \end{bmatrix}, R_\theta = \begin{bmatrix} \cos\theta & 0 & \sin\theta \\ 0 & 1 & 0 \\ -\sin\theta & 0 & \cos\theta \end{bmatrix}, R_\varphi = \begin{bmatrix} \cos\varphi & -\sin\varphi & 0 \\ \sin\varphi & \cos\varphi & 0 \\ 0 & 0 & 1 \end{bmatrix}. \quad (1)$$

For simplicity, we let $R(\Omega) = R_\phi R_\theta R_\varphi$. In addition, we used the location of the sensor relative to the central pivot point of the drone, defined by

$$\mathbf{r} = [l, 0, h]^T, \quad (2)$$

where l and h are the distance in length and height the sensor is located away from the center of the sUAS, as shown in Figure 4.

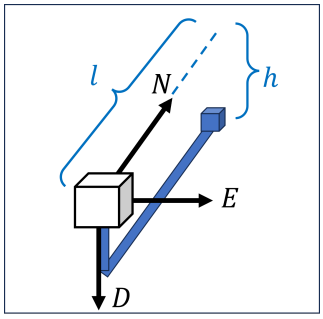

Figure 4. This diagram depicts the center of the sUAS (white box) with the TriSonica sensor (blue box) located out front of the aircraft, as described in Equation (2). The north-east-down (NED) coordinates (i.e., the $\hat{\mathbf{e}}_d$ basis shown in Figure 3) describe the location relative to the center of the sUAS.

We separated the three corrections into different cases. In Correction 1 (C1), the raw measured wind speed vector is only subject to heading-based and pose corrections:

$$\hat{\mathbf{u}}_m(k\Delta t) = R(\Omega)\mathbf{u}_m(k\Delta t). \quad (3)$$

In Correction 2 (C2), the estimate is further corrected by adjusting for the vehicle's induced translational velocity:

$$\hat{\mathbf{u}}_m(k\Delta t) = R(\Omega)(\mathbf{u}_m(k\Delta t) - \mathbf{v}(k\Delta t)). \tag{4}$$

In Correction 3 (C3), the vehicle's induced rotational velocity is adjusted using the gyroscope data and the sensor position:

$$\hat{\mathbf{u}}_m(k\Delta t) = R(\Omega)(\mathbf{u}_m(k\Delta t) - \mathbf{v}(k\Delta t) - \mathbf{v}_r(k\Delta t)), \tag{5}$$

where $\mathbf{v}_r = \mathbf{r} \times \dot{\Omega}$.

2.4.2. Filtering

In an effort to determine how wind speed values were affected by sUAS flight parameters, we considered major factors that could impact the free air stream flow into the TriSonica sensor. We hypothesized that the propellers and orientation of the aircraft (relative to the mean wind direction) were the most dominant. Therefore, we chose to filter the data in three primary ways (see Figure 5). The first was by sUAS velocity (ms^{-1}). We expected wind speed measurement values to be negatively impacted when the sUAS was changing direction due to slow speeds and ascending in place, which would increase local turbulence and propeller induced bias into the sensor (no measurements were performed while descending). The second was by the relative angle difference between the heading of the aircraft and the mean wind direction, $\Delta\varphi$ (with respect to the Tower). We were curious whether data accuracy would be effected by this angle size, as it relates to the location of the sensor within the free air stream. We experimented with various angles to find the one that provided the most reliable results. We then filtered the data a third way, considering the relative difference between the vector describing the direction of travel (i.e., velocity vector) and the heading vector. When the sUAS heading is perpendicular to the direction of travel, the free air stream is obstructed by the propeller intake air flow. Therefore, we filtered the data such that sUAS velocity values, $\mathbf{v}$, below 1 ms^{-1} were removed. The data were further filtered by removing any data where the angle size $\Delta\varphi$ was greater than $\pm 20°$. Lastly, we removed any data where the difference between heading vector and velocity vector, β, was greater than $\pm 20°$. To verify the validity of these filtering parameter values, the Tower measurements were used as our ground truth estimate. We reserved the optimal choice of filtering parameters for future work, which may depend heavily on sensor placement and environmental conditions and need to be validated in controlled conditions (i.e., wind tunnel test, etc).

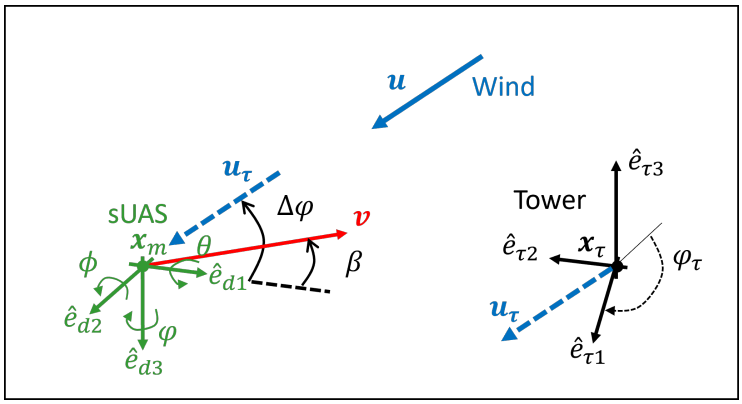

Figure 5. The TriSonica filtering variables based on velocity ($\mathbf{v}$), the relative angle difference between the aircraft heading and mean wind direction ($\Delta\varphi$), and the relative difference between the direction of travel and sUAS heading (β). $\Delta\varphi$ is computed with respect to the Tower wind measurement, $\mathbf{u}_\tau$, which is assumed to be the closest measurement to the true wind vector $\mathbf{u} \approx \mathbf{u}_\tau$.

3. Results

3.1. AirMar vs. Tower

To understand how differences in sUAS- vs. Tower-based wind measurements may be influenced by the fact that these two measurements are not co-located, we compared wind measurements using an AirMar sensor placed both next to the Tower (co-located) and approximately 22 m away (separated), on the edge of the bog (Figure 1). We found that when the AirMar sensor was co-located, there was on average 0.51 and 0.45 ms^{-1} discrepancy between the Tower for the u_{a_1} and u_{a_2} components, respectively (Figure 6). This difference increased to 0.72 and 0.61 ms^{-1} when the AirMar was no longer co-located. The spread of these differences, as represented by the 95% confidence interval, was also higher when the two sensors were separated.

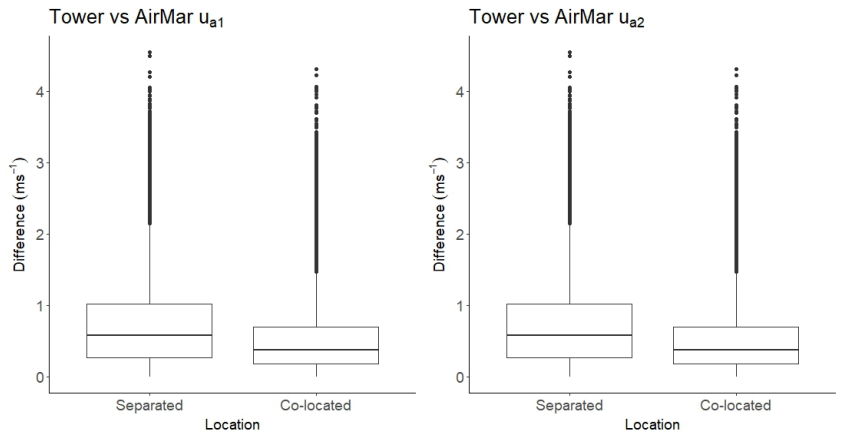

Figure 6. The difference between the Tower (gold standard sensor) versus the AirMar (stand-alone sensor) u_{a_1} and u_{a_2} wind components, depending on if the AirMar was co-located versus separated by about 22 m (see Figure 1). Boxes represent the 25th and 75th percentiles, the bar within shows the median. Whiskers are 1.5× the inter-quartile range.

3.2. TriSonica vs. Tower

We compared the sUAS-based TriSonica wind measurements to the Tower wind data to understand how post-flight filtering and data corrections influence sUAS-based wind speed and direction data. Results are presented in the following ways: (1) TriSonica data that were subject to filtering, as described in Section 2.4.2, compared to non-filtered data; (2) TriSonica data subject to corrections (i.e., C1, C2, and C3; see Section 2.4.1) compared to data without corrections (labeled NC); (3) postulating that due to terrain differences (Figure 1) the wind of the E-W flights may need to travel over more trees compared to the N-S flights, increasing turbulence and boundary layer effects; we examined the N-S and E-W flight data separately, and (4) to establish a baseline, we added the comparison between the AirMar and Tower wind data for both filtered and non-filtered data (filtering with respect to the TriSonica). The AirMar data include flights where this sensor was both co-located and separated from the Tower. The average wind speeds of the Tower for all flights, both filtered and unfiltered, are shown in Table 1. The error between wind speed of the Tower and the TriSonica are given in terms of relative error, $100(|u_m| - |u_\tau|)/|u_\tau|$.

When considering all of the flight data together (i.e., both N-S and E-W transects) to compare the different levels of corrections (see Figure 7) we found that

- the AirMar measurement has a median wind speed error of 23% and wind direction error of $25^\circ \pm 13$;
- the TriSonica wind speed errors are very similar between when the data are not corrected (NC, 36%) and the three corrections (C1–C3; 36%, 45%, and 45%, respectively);

- the TriSonica wind direction error for the NC and C1 cases have the highest median values (91° ± 47° and 108° ± 39°, respectively) and variability with respect to outliers (from 120% to 200%+).

Table 1. A comparison between the filtered average wind speed data (see Section 2.4.2) from the tower and the raw (unfiltered) tower data during the different flights (f#) in ms^{-1}. The N-S flights consist of f1, f2, f7 and f8, and the E-W flights consist of f3–f6.

Flight Number	Avg Tower (Filt)	Std Tower (Filt)	Avg Tower (Raw)	Std Tower (Raw)
f1	2.53	0.47	2.97	0.90
f2	1.34	0.74	2.84	0.89
f3	2.04	0.69	1.76	0.69
f4	1.28	0.41	1.16	0.45
f5	1.70	0.52	1.33	0.68
f6	1.01	0.68	1.14	0.52
f7	1.84	0.29	1.96	0.46
f8	2.13	0.44	1.69	0.81

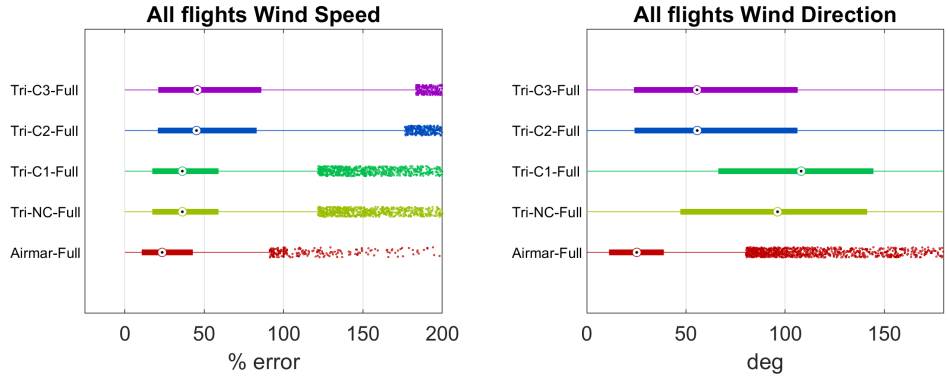

Figure 7. The wind correction results are shown for all data collected (i.e., no filtering or separating flights by transect orientation) in a horizontal box plot. The circle with a dot represents the median, the box shows the quartiles, the whiskers the minimum and maximum values, and the dots represent outliers.

When examining the wind speed data for the N-S and E-W flights separately (Figure 8a,b), we observed that

- The N-S median TriSonica (all correction levels) and AirMar wind speed data, both with and without filtering, are very similar, with values ranging from 18 to 30%;
- The E-W median value of the AirMar, 21–23%, is substantially lower than any of the TriSonica corrected data, both with and without filtering (50–55%);
- The unfiltered N-S and E-W flights have considerably more outliers compared to filtered data. The AirMar data also show some outliers in the unfiltered case, however not at the magnitude of the TriSonica data.

Conversely, if we consider wind direction for the N-S and E-W flights (Figure 8c,d), we observe the following:

- The N-S and E-W median wind direction values for the NC and C1 cases (both filtered and unfiltered) show little similarity to the Tower or AirMar data.
- The N-S wind direction median values for the C2 and C3 unfiltered cases, 118° and C3, 117°, respectively, show large increases in error.
- The N-S wind direction median values for the C2 and C3 filtered values, 30° and 31°, respectively, show large decreases in error compared to unfiltered values.

- The E-W wind direction median values for the C2 and C3 unfiltered cases, 41° and 41°, respectively, show similar error compared to the AirMar (31°) but contain more variability (18°–73° versus 20°–44°, respectively).
- The variability for filtered C2 and C3 E-W wind directions (20°–61°) is much smaller than the unfiltered cases for C2 and C3 (18°–73°). The filtered C2 and C3 values are similar to those of the AirMar (24°–46°).

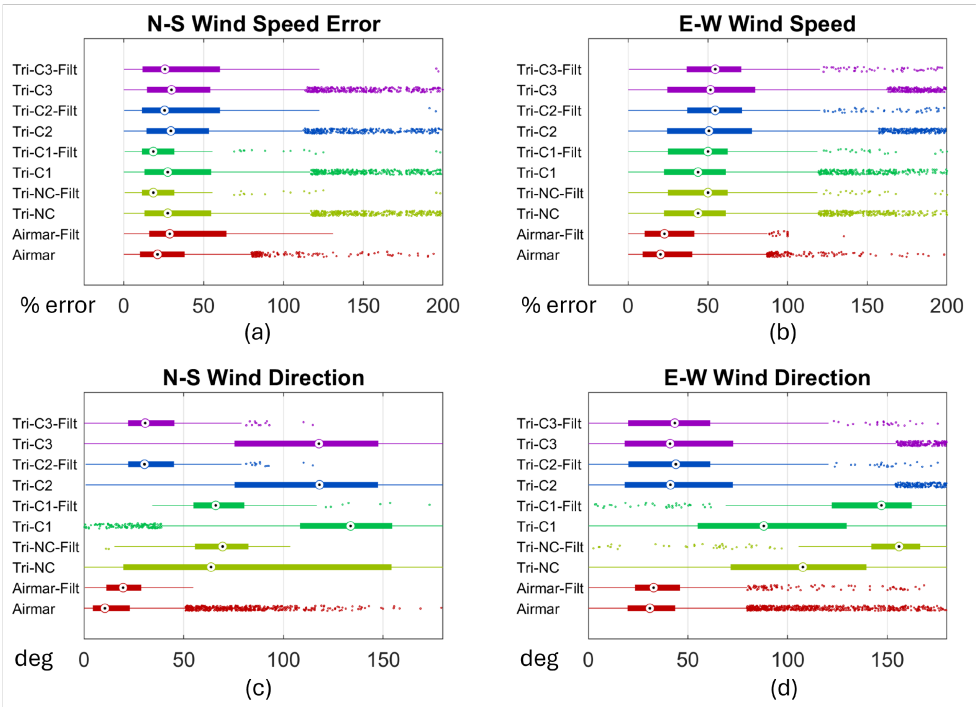

Figure 8. Correction and filtering results for N-S flights and E-W flights for errors in wind speed ((**a**,**b**), respectively) and wind direction ((**c**,**d**), respectively) are shown in a horizontal box plot. The circle with a dot represents the median, the box shows the quartiles, the whiskers the minimum and maximum values, and the dots represent outliers. All data are presented with respect to the Tower data. The y-axis indicates the type of data corrections applied (outlined in Section 2.4.1) and whether they are filtered (described in Section 2.4.2). Additionally, for comparison, the AirMar data are shown as a baseline.

Given the differences between the N-S and E-W flights, we wondered whether atmospheric stability was impacting the ability to measure wind data onboard the sUAS. To test this idea, we utilized two metrics to describe the wind behavior during the flight, turbulence intensity, τ_i, and the normalized standard deviation of the wind direction, $\tau_\theta = \sigma_\theta/360$. We defined turbulence intensity (with respect to the Tower measurements) as the standard deviation of the wind speed magnitude, σ_u, divided by the mean wind speed magnitude, $\overline{u}_t$, such that $\tau_i = \sigma_u/\overline{u}_t$. When the turbulence intensity (τ_i) value is small (i.e., close to zero), there is little to no turbulence, which means the wind is more stable and less variable. Conversely, if the value is larger (closer to 1), the turbulence is greater. When we plot the average errors in wind speed against τ_i and τ_θ (Figure 9), we see that both the wind speed error (color bar) and spread of this error diminish as turbulence intensity (τ_i) and the standard deviation of the wind direction (τ_θ) decrease. The relationship between these values and wind direction error is less compelling (Figure 9). To further examine these factors, we plotted turbulence intensity (τ_i) against the average and standard deviation of the error for wind speed (Figure 10). As expected, we found that as we have more stable wind (lower turbulence intensity), we observe lower average errors in wind speed as well as lower variability for this error. We also examined (τ_θ) against the average error for wind direction and found no correlation (correlation coefficient = 0.06) (data not shown).

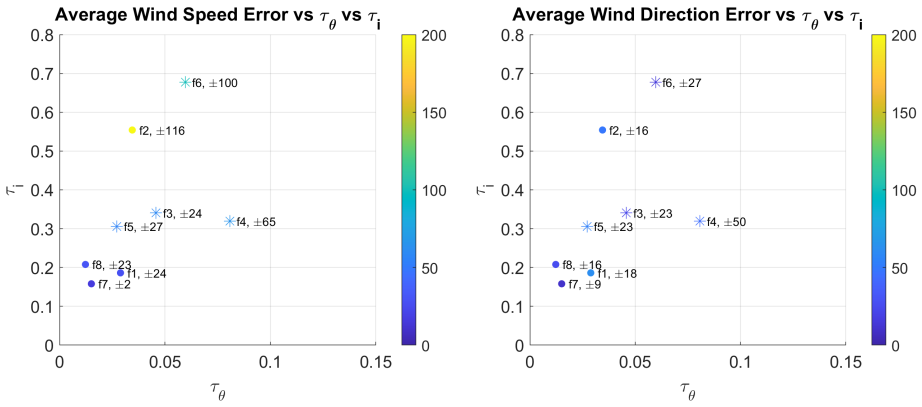

Figure 9. Plotting average TriSonica wind speed % error (value represented in color) by turbulence intensity (τ_i) and normalized standard deviation of wind direction (τ_θ) show that when conditions are stable TriSonica measurements that were filtered and corrected can perform quite well compared to Tower measurements. Flight numbers (f#) and standard deviation of % error are listed for each flight. North-south flight numbers are 1, 2, 7, and 8; east-west flight numbers are 3–6.

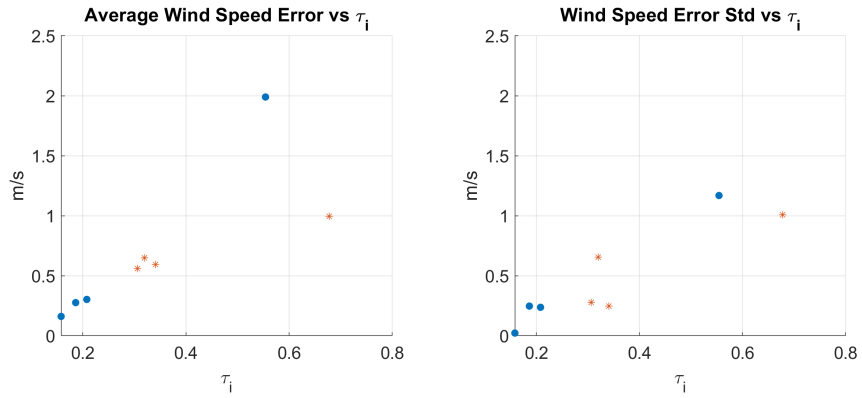

Figure 10. Relationship between τ_i and average and standard deviation wind speed error. Data are filtered and corrected. Correlation coefficients are 0.79 and 0.90, respectively. Blue circles represent N-S flights, while orange colors represent E-W flights.

4. Discussion

4.1. Effects of Separation on Wind Data

The sUAS-based measurements we examine in this study are never truly collocated with our reference sensor, the Tower. As such, some of the error in our comparison of these two data sources are due to fluctuations in the wind field in these different locations. To examine how this spatial separation might influence our results, we placed an additional wind sensor, the AirMar, both next to and 22 m away from the Tower. We found that separation of the instruments added 0.16–0.21 ms^{-1} of error. Considering that at times the errors between the filtered/corrected TriSonica measurements and the AirMar measurements were similar in magnitude (Figure 8), it can be postulated that under proper relative wind speed conditions and sUAS orientation the mobile onboard measurements are no less accurate than fixed measurements taken in a different location.

4.2. Filtering and Correcting Aerial Data

Many conditions (e.g., weather, flight parameters, relative wind speed over the sensor) need to optimized in order for aerial wind measurements to replicate the true signal. Previous studies where a TriSonica was used to measure wind speed found differences in wind speed between the sensor and reference measurements between 20

and 50% ([26] examining experiments by [37], [25]). Both of these studies mounted the TriSonica above the sUAS, which may increase errors, especially at low wind speeds [31]. It is also important to note that both of these studies had the sUAS in a fixed location, which reduces the relative wind speed over the TriSonica sensor.

sUAS-based wind measurements include other types of error (such as sensor noise, propeller induced biases, and correction inconsistencies); we set about quantifying the impact of some of those factors. Some of the errors seen in our data can be attributed to low true wind speeds. Low wind speeds, combined with the limitations of the TriSonica (which has stated u/v accuracy of ± 0.10 ms^{-1}) and translational velocities of $\approx$1.5–2 ms^{-1}, are the likely explanation as to why our average wind speed error is on the order of 1 ms^{-1} in the not corrected (NC) case. We also wanted to understand more about variability within our filtered and corrected data. For this examination, we processed these data using a Savitzky-Golay filter over a 2 s interval and examined the resulting variabilities. When applying this process to the TriSonica data, we found a wind speed deviation ($\delta|u_m|$) of 0.07 ms^{-1}, which is similar to the stated accuracy of this sensor. We also used this filtering approach to examine errors related to the sUAS. Translational velocity ($\delta|v|$) had deviations of 0.03 ms^{-1}. Pose ($\delta\Omega$; pitch, roll, and yaw) had deviations of $[1.9, 1.1, 14.9]^\circ$, respectively, while rotational rates ($\delta\dot{\Omega}$; pitch rate, roll rate, and yaw rate) had deviations of $[0.14, 0.83, 0.36]^\circ$ s^{-1}, respectively. By utilizing Equation (5), the deviations of the TriSonica measurement, translational velocity, pose, and rotational rate can be converted to ms^{-1} using a sequential perturbation method, resulting in an estimated total uncertainty of around ± 0.14 ms^{-1}. Of this value, the TriSonica contributes the majority of the uncertainty (>80%). The remaining uncertainty lies within the translational velocity (16%), with very little from rotation rates (3%) and pose (<0.01%). It should be noted that this simple test of uncertainty propagation does not include the bias and variability induced by the aircraft.

Our observations give clear indications that both corrections and filtering are needed, especially for more accurate wind direction data (Section 3.2, Figure 8). Our results also indicate that the translational velocity corrections (C2) are the most effective for calculating the true wind direction signal. Improvements due to the rotational velocity corrections (C3) were minor and inconclusive; this result is likely due to the fact that rotational impacts while flying the main section of each transect are small. The sections most impacted by rotational effects are the ends of the transects, where the sUAS turns and adjusts its altitude. Our filtering criteria (Section 2.4.2) excluded the end of each transect, where this process occurs, due to concerns regarding the influence of propeller wash on both the wind and methane measurements while the sUAS was turning and ascending. If one needed to also include transect ends in their data stream, additional investigation into the impacts of the C2 to C3 correction would be needed. However, we do not recommend including the end sections of transects. Our results indicate that wind speed and direction errors are substantially larger without filtering the data for velocity ($\mathbf{v}$; Section 2.4.2), relative angle differences ($\Delta\varphi$), and the difference between the sUAS heading and wind direction (β). We suspect that these filtering criteria may be dependent somewhat on sensor placement relative to the propeller geometry, which in turn impacts the effects of prop wash.

We also found that reduced turbulence intensity (τ_i) and less variability in wind direction (τ_θ) helped reduce errors in wind speed, and, to a lesser effect, wind direction (Figure 9). Therefore, flying during times when atmospheric stability is at a maximum would aid in obtaining more accurate sUAS-based wind measurements. However, it is unrealistic to expect flights to occur only during optimal atmospheric conditions. We suggest instead users should focus on increasing localized wind stability. Air stability around a sUAS-based wind sensor is influenced by the aircraft propulsion system, the sUAS heading, as well as wind speed and direction.

In N-S flights, most of the wind speed measurements were near or above 2 ms^{-1} (Table 1). In contrast, in all E-W flights, with the exception of Flight 3, the wind speed stayed under 2 ms^{-1}. These differences could be one explanation as to why our results differ depending on transect orientation. To examine this concept further, we plotted wind speed and wind direction error as a function of relative wind speed for both transects. We found that wind speed errors diminish as relative wind speed increases (Figure 11A), with more measurements having errors < 1 ms^{-1} when relative wind speeds reach 2.5 ms^{-1} or greater (Figure 11B). This value is similar to 2.3 ms^{-1} found in [23], below which authors found increased errors in sUAS-based emissions. Trends with wind direction errors are less clear, although these errors do diminish somewhat at relative wind speeds greater than 3.5 ms^{-1} (Figure 11C,D). Based on these results, we believe that flight planning to increase the time that sensors are in relatively free air streams could be an effective tool to minimize wind speed and direction measurement errors. Utilizing the wind triangle (Figure 12), whereby flights are flown in a manner to maximize relative wind speed (red arrow), during this planning should positively impact the accuracy of both wind speed and direction measurements. Investigating the ability to optimize relative wind speeds utilizing the wind triangle is a logical next step for future investigations. In addition, further studies could examine the relative wind speed needed for reduced measurement errors. Potential reasons we found smaller wind speed errors at or above relative wind speeds of 2.5 ms^{-1} could be lower turbulence intensity and/or greater atmospheric stability above this value. Understanding the factors controlling this value and how it may vary with different platform/sensor configurations, environmental conditions, and terrain would greatly inform future missions.

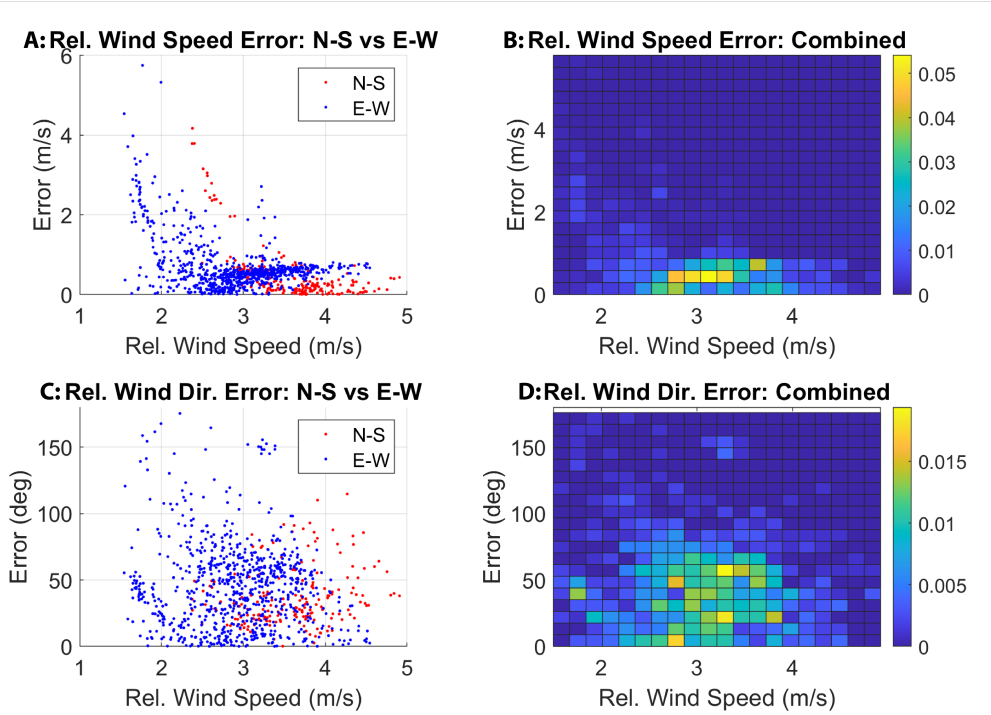

Figure 11. Errors for wind speed and wind direction plotted against relative wind speed of sUAS-mounted sensor. Panels (**A**,**C**) show data separated by N-S and E-W flights. Panels (**B**,**D**) show all data combined with colors representing percentage of data meeting those criteria. All plots show decreased errors as relative wind speed increases. All data are filtered and corrected.

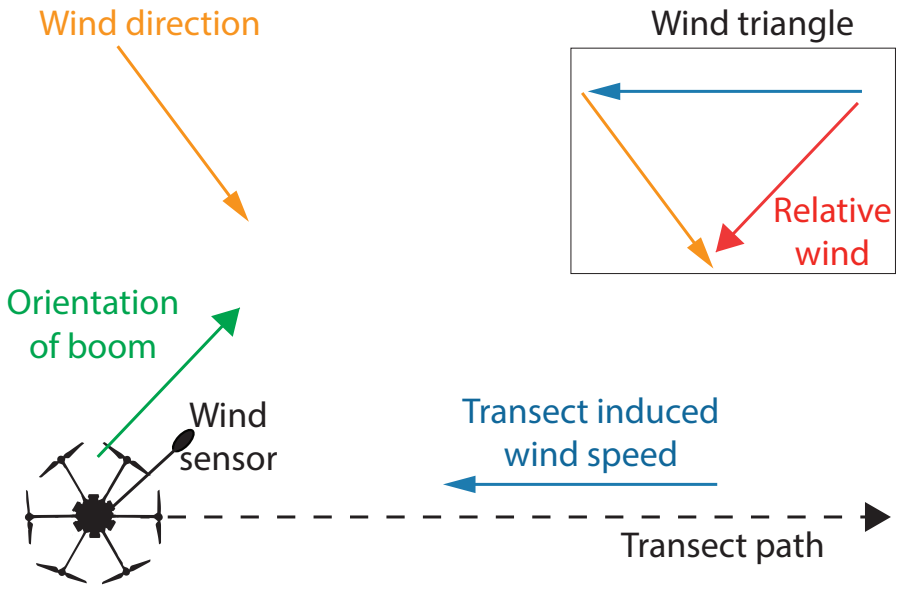

Figure 12. A diagram depicting a strategy for measuring joust configured wind measurements. Using wind triangle concept, one can maximize free air flow of wind sensor if orientation of wind sensor on boom (green arrow) can match that of relative wind direction (red arrow). Components of wind triangle are transect-induced wind speed (blue arrow) and wind direction (orange arrow).

5. Conclusions

In this work, we explored the conditions necessary for accurate sUAS-based wind measurements by evaluating different levels of corrections (i.e., pose and induced velocities from translation and rotation) and filtering (i.e., aircraft heading and velocity relative to the true wind direction) for specific flight conditions. Our tests were conducted with the wind sensor placed in the joust configuration with transects flown as curtains such that gas emissions (in our case methane) could be determined using the mass balance method. We found that filtering greatly reduced the number of observations with very high wind speed errors. Combining filtering with corrections, especially those for transitional velocity, reduced errors in wind direction measurements from 50° to >125° to 20–30°. The range of the errors we saw varied depending on the correction level applied and transect orientation (N-S vs. E-W). The importance of transect orientation is likely related to the different wind speeds found between these two sets of measurements. A simple uncertainty propagation analysis using the Savitzky–Golay filter, which looked at the deviations from the correction inputs, found that the TriSonica contributed a large portion of the uncertainty in the measurement (>80%). These errors are also likely due to low true wind speeds, which, when combined with the limitations of the TriSonica's accuracy (stated as ± 0.1 ms^{-1}), created large relative errors. Based on our ground-based sensor comparisons (an AirMar co-located and separated from the Tower), little error, $\approx$0.1–0.2 ms^{-1}, is due to the fact that the Tower and sUAS measurements are not co-located. We also found that wind speed errors decreased with lower turbulence intensity and higher relative wind speeds (>2.5 ms^{-1}). Although we did not see a relationship between turbulence intensity and errors in wind direction, we did observe some loose trends where wind direction errors were diminished at higher relative wind speeds (>3.5 ms^{-1}). As such, flight planning could be used to minimize errors in wind speed and, to a lesser effect, wind direction. Future work should continue investigating optimal flight conditions for sUAS-based wind speed and direction measurements (e.g., optimum relative wind speeds, location of the sensor, orientation of the sensor during flight, etc.).

Author Contributions: Conceptualization: K.M.; data acquisition: K.M. and C.E.; data processing: D.H., C.E. and K.M.; writing—original draft preparation: D.H. and K.M.; writing—review and editing: K.M., D.H., C.E. and E.E.; funding acquisition: K.M. and E.E. All authors have read and agreed to the published version of the manuscript.

Funding: This research was funded in part by the U.S. Geological Survey Land Change Science Program in the Ecosystems Mission Area. D.H. was supported by the Center for Methane Emissions Research and Innovation (CMERI) funded by the University of California Merced Climate Action Seed Funds grant. Support was also provided by National Science Foundation Grants DEB LTREB 1354370 and 2011257.

Data Availability Statement: The data used in this work can be found at doi:10.5066/P142EBC3.

Acknowledgments: We acknowledge the assistance of the U.S. Geological Survey Fairbanks office, the U.S. Geological National Uncrewed Systems Office (NUSO), and the Bonanza Creek LTER, without which this work would not be possible. Any use of trade, firm, or product names is for descriptive purposes only and does not imply endorsement by the U.S. Government.

Conflicts of Interest: The authors declare no conflicts of interest.

Abbreviations

The following abbreviations are used in this manuscript:

C#	Correction number
E-W	East–west
GHG	Greenhouse gas
GPS	Global positioning system
IMU	Inertial measurement unit
IPCC	Intergovernmental Panel on Climate Change
M600	Matrice 600
NC	No correction
N-S	North–south
OTM	Other test method
sUAS	Small uncrewed aircraft system

References

1. Lee, H.; Romero, J. (Eds.). *IPCC, 2023: Climate Change 2023: Synthesis Report. Contribution of Working Groups I, II and III to the Sixth Assessment Report of the Intergovernmental Panel on Climate Change*; IPCC: Geneva, Switzerland, 2023; 184p. [CrossRef]
2. U.S. Environmental Protection Agency. *Inventory of U.S. Greenhouse Gas Emissions and Sinks: 1990–2021*; U.S. Environmental Protection Agency: Washington, DC, USA, 2023.
3. Burgués, J.; Marco, S. Environmental chemical sensing using small drones: A review. *Sci. Total Environ.* **2020**, *748*, 141172. [CrossRef]
4. Zhu, Z.; González-Rocha, J.; Ding, Y.; Frausto-Vicencio, I.; Heerah, S.; Venkatram, A.; Dubey, M.; Collins, D.; Hopkins, F. Toward on-demand measurements of greenhouse gas emissions using an uncrewed aircraft Aircore system. *EGUsphere* **2023**, *2023*, 1–23. [CrossRef]
5. Leitner, S.; Feichtinger, W.; Mayer, S.; Mayer, F.; Krompetz, D.; Hood-Nowotny, R.; Watzinger, A. UAV-based sampling systems to analyse greenhouse gases and volatile organic compounds encompassing compound-specific stable isotope analysis. *Atmos. Meas. Tech.* **2023**, *16*, 513–527. [CrossRef]
6. Gullett, B.; Aurell, J.; Mitchell, W.; Richardson, J. Use of an unmanned aircraft system to quantify NO_x emissions from a natural gas boiler. *Atmos. Meas. Tech.* **2021**, *14*, 975–981. [CrossRef] [PubMed]
7. Hollenbeck, D.; Zulevic, D.; Chen, Y. Advanced leak detection and quantification of methane emissions using suas. *Drones* **2021**, *5*, 117. [CrossRef]
8. Yang, S.; Talbot, R.W.; Frish, M.B.; Golston, L.M.; Aubut, N.F.; Zondlo, M.A.; Gretencord, C.; McSpiritt, J. Natural Gas Fugitive Leak Detection Using an Unmanned Aerial Vehicle: Measurement System Description and Mass Balance Approach. *Atmosphere* **2018**, *9*, 383. [CrossRef]
9. Corbett, A.; Smith, B. A study of a miniature TDLAS system onboard two unmanned aircraft to independently quantify methane emissions from oil and gas production assets and other industrial emitters. *Atmosphere* **2022**, *13*, 804. [CrossRef]

10. Smith, B.; Buckingham, S.; Touzel, D.; Corbett, A.; Tavner, C. Development of Methods for Top-Down Methane Emission Measurements of Oil and Gas Facilities in an Offshore Environment Using a Miniature Methane Spectrometer and Long-Endurance UAS. In Proceedings of the SPE Annual Technical Conference and Exhibition, SPE, Dubai, United Arab Emirates, 21–23 September 2021; p. D031S047R006.
11. Environmental Protection Agency. Other Test Method 51 (OTM-51)—UAS Application of Method 21 for Surface Emission Monitoring of Landfills. 2022. Available online: https://www.epa.gov/system/files/documents/2022-12/OTM%2051-%20UAS%20Application%20of%20Method%2021%20for%20Surface%20Emission%20Monitoring%20of%20Landfills.pdf (accessed on 12 March 2024).
12. Olaguer, E.P.; Jeltema, S.; Gauthier, T.; Jermalowicz, D.; Ostaszewski, A.; Batterman, S.; Xia, T.; Raneses, J.; Kovalchick, M.; Miller, S.; et al. Landfill Emissions of Methane Inferred from Unmanned Aerial Vehicle and Mobile Ground Measurements. *Atmosphere* **2022**, *13*, 983. [CrossRef]
13. Abichou, T.; Bel Hadj Ali, N.; Amankwah, S.; Green, R.; Howarth, E.S. Using Ground-and Drone-Based Surface Emission Monitoring (SEM) Data to Locate and Infer Landfill Methane Emissions. *Methane* **2023**, *2*, 440–451. [CrossRef]
14. Hintsa, E.J.; Moore, F.L.; Hurst, D.F.; Dutton, G.S.; Hall, B.D.; Nance, J.D.; Miller, B.R.; Montzka, S.A.; Wolton, L.P.; McClure-Begley, A.; et al. UAS Chromatograph for Atmospheric Trace Species (UCATS)—A versatile instrument for trace gas measurements on airborne platforms. *Atmos. Meas. Tech.* **2021**, *14*, 6795–6819. [CrossRef]
15. Wu, C.; Liu, B.; Wu, D.; Yang, H.; Mao, X.; Tan, J.; Liang, Y.; Sun, J.Y.; Xia, R.; Sun, J.; et al. Vertical profiling of black carbon and ozone using a multicopter unmanned aerial vehicle (UAV) in urban Shenzhen of South China. *Sci. Total Environ.* **2021**, *801*, 149689. [CrossRef] [PubMed]
16. Tsunogai, U.; Shingubara, R.; Morishita, Y.; Ito, M.; Nakagawa, F.; Yoshikawa, S.; Utsugi, M.; Yokoo, A. Sampling Volcanic Plume Using a Drone-Borne SelPS for Remotely Determined Stable Isotopic Compositions of Fumarolic Carbon Dioxide. *Front. Earth Sci.* **2022**, *10* . [CrossRef]
17. Galle, B.; Arellano, S.; Bobrowski, N.; Conde, V.; Fischer, T.P.; Gerdes, G.; Gutmann, A.; Hoffmann, T.; Itikarai, I.; Krejci, T.; et al. A multi-purpose, multi-rotor drone system for long-range and high-altitude volcanic gas plume measurements. *Atmos. Meas. Tech.* **2021**, *14*, 4255–4277. [CrossRef]
18. Rea-Downing, G.; Bouligand, C.; Glen, J.; Earney, T.; Zielinski, L.; Anderson, J.E.; Kelly, P. Development of small uncrewed aerial systems for multi-instrument geophysical data acquisition in active geothermal systems. In Proceedings of the Summit on Drone Geophysics ; Society of Exploration Geophysicists: Houston, TX, USA, 2023.
19. Aurell, J.; Gullett, B.; Holder, A.; Kiros, F.; Mitchell, W.; Watts, A.; Ottmar, R. Wildland fire emission sampling at Fishlake National Forest, Utah using an unmanned aircraft system. *Atmos. Environ.* **2021**, *247*, 118193. [CrossRef] [PubMed]
20. Keerthinathan, P.; Amarasingam, N.; Hamilton, G.; Gonzalez, F. Exploring unmanned aerial systems operations in wildfire management: data types, processing algorithms and navigation. *Int. J. Remote Sens.* **2023**, *44*, 5628–5685. [CrossRef]
21. Manies, K.; Yates, E.; Christensen, L.; Kolyer, R.; Euskirchen, E.; Waldrop, M. Can a drone equipped with a miniature methane sensor determine methane fluxes from an Alaskan wetland? In Proceedings of the AGU Fall Meeting Abstracts ; Washington, DC, USA, 2018; p. B41H-2809.
22. Hollenbeck, D.; Manies, K.; Chen, Y.; Baldocchi, D.D.; Euskirchen, E.S.; Christensen, L. Evaluating a UAV-based mobile sensing system designed to quantify ecosystem-based methane. In Proceedings of the AGU Fall Meeting Abstracts ; Online 2020; p. A115-0007.
23. Morales, R.; Ravelid, J.; Vinkovic, K.; Korbeń, P.; Tuzson, B.; Emmenegger, L.; Chen, H.; Schmidt, M.; Humbel, S.; Brunner, D. Controlled-release experiment to investigate uncertainties in UAV-based emission quantification for methane point sources. *Atmos. Meas. Tech.* **2022**, *15*, 2177–2198. [CrossRef]
24. EPA. Draft Other Test Method 33A: Geospatial Measurement of Air Pollution, Remote Emissions Quantification—Direct Assessment (GMAP-REQ-DA). Environmental Protection Agency (EPA). 2014. Available online: https://www3.epa.gov/ttnemc01/prelim/otm33a.pdf (accessed on 21 January 2025).
25. Hollenbeck, D.; Nunez, G.; Christensen, L.E.; Chen, Y. Wind measurement and estimation with small unmanned aerial systems (suas) using on-board mini ultrasonic anemometers. In Proceedings of the 2018 International Conference on Unmanned Aircraft Systems (ICUAS), Dallas, TX, USA, 12–15 June 2018; pp. 285–292.
26. Thielicke, W.; Hübert, W.; Müller, U.; Eggert, M.; Wilhelm, P. Towards accurate and practical drone-based wind measurements with an ultrasonic anemometer. *Atmos. Meas. Tech.* **2021**, *14*, 1303–1318. [CrossRef]
27. Prudden, S.; Fisher, A.; Marino, M.; Mohamed, A.; Watkins, S.; Wild, G. Measuring wind with small unmanned aircraft systems. *J. Wind. Eng. Ind. Aerodyn.* **2018**, *176*, 197–210. [CrossRef]
28. Brenner, J. Inflow Analysis for Multi-Rotors and the Impact on Sensor Placement. Master's Thesis, Oklahoma State University, Stillwater, OK, USA, 2019.
29. González-Rocha, J.; Woolsey, C.A.; Sultan, C.; De Wekker, S.F. Sensing wind from quadrotor motion. *J. Guid. Control. Dyn.* **2019**, *42*, 836–852. [CrossRef]

30. Abichandani, P.; Lobo, D.; Ford, G.; Bucci, D.; Kam, M. Wind Measurement and Simulation Techniques in Multi-Rotor Small Unmanned Aerial Vehicles. *IEEE Access* **2020**, *8*, 54910–54927. [CrossRef]
31. Chiew, J.; Aftosmis, M.; Manies, K.L. Medium-Fidelity CFD Modeling of Multicopter Wakes for Airborne Sensor Measurements. In Proceedings of the 78th Annual Vertical Flight Society Forum and Technology Display, Fort Worth, TX, USA, 10–12 May 2022.
32. Manies, K.L.; Jones, M.C.; Waldrop, M.P.; Leewis, M.C.; Fuller, C.; Cornman, R.S.; Hoefke, K. Influence of Permafrost Type and Site History on Losses of Permafrost Carbon After Thaw. *J. Geophys. Res. Biogeosci.* **2021**, *126*, e2021JG006396, [CrossRef]
33. Euskirchen, E.S.; Edgar, C.W.; Turetsky, M.R.; Waldrop, M.P.; Harden, J.W. Differential response of carbon fluxes to climate in three peatland ecosystems that vary in the presence and stability of permafrost. *J. Geophys. Res. Biogeosci.* **2014**, *119*, 1576–1595. [CrossRef]
34. Burgués, J.; Marco, S. Drone-based monitoring of environmental gases. In *Air Quality Networks: Data Analysis, Calibration & Data Fusion*; Springer: Switzerland, 2023; pp. 115–137.
35. Asher, E.; Hills, A.J.; Hornbrook, R.S.; Shertz, S.; Gabbard, S.; Stephens, B.B.; Helmig, D.; Apel, E.C. Unpiloted aircraft system instrument for the rapid collection of whole air samples and measurements for environmental monitoring and air quality studies. *Environ. Sci. Technol.* **2021**, *55*, 5657–5667. [CrossRef] [PubMed]
36. Smith, B.; John, G.; Stark, B.; Christensen, L.E.; Chen, Y. Applicability of unmanned aerial systems for leak detection. In Proceedings of the 2016 International Conference on Unmanned Aircraft Systems (ICUAS), Arlington, VA, USA, 7–10 June 2016; pp. 1220–1227.
37. Donnell, G.W.; Feight, J.A.; Lannan, N.; Jacob, J.D. Wind characterization using onboard IMU of sUAS. In Proceedings of the 2018 Atmospheric Flight Mechanics Conference, Atlanta, GA, USA, 25–29 June 2018; p. 2986.

Disclaimer/Publisher's Note: The statements, opinions and data contained in all publications are solely those of the individual author(s) and contributor(s) and not of MDPI and/or the editor(s). MDPI and/or the editor(s) disclaim responsibility for any injury to people or property resulting from any ideas, methods, instructions or products referred to in the content.